


 Cite this: *RSC Adv.*, 2025, **15**, 19348

# Tunable color, optical properties, and energy transfer of $\text{Tb}^{3+}$ – $\text{Sm}^{3+}$ – $\text{Yb}^{3+}$ tri-doped lithium–niobium–tellurite glass for applications in color display devices and WLEDs<sup>†</sup>

Ho Kim Dan, <sup>a,b</sup> Nguyen Dinh Trung, <sup>c</sup> Nguyen Minh Tam, <sup>d</sup> L. T. Ha, <sup>e</sup> Vu Thi Kim Lien, <sup>\*fg</sup> D. T. Khan, <sup>h</sup> Nguyen Le Thai, <sup>i</sup> Dacheng Zhou<sup>j</sup> and Jianbei Qiu<sup>j</sup>

A  $\text{TeO}_2$ – $\text{Nb}_2\text{O}_5$ – $\text{LiO}_2$ – $\text{CaO}$  (TNLC) lithium–niobium–tellurite glass single-doped and co-doped with  $\text{Tb}^{3+}$ ,  $\text{Sm}^{3+}$ , and  $\text{Yb}^{3+}$  ions was synthesized via a conventional melt-quenching method. The  $\text{Tb}^{3+}$ – $\text{Sm}^{3+}$  co-doped TNLC glass could be tuned to emit white light effectively by controlling the ratio of  $\text{Tb}^{3+}$  and  $\text{Sm}^{3+}$  in the glass. The fluorescence lifetime of the  $\text{Tb}^{3+}$ – $\text{Sm}^{3+}$  co-doped TNLC glass indicated the existence of multiple energy transfer channels, including from  $\text{Tb}^{3+}$  to  $\text{Sm}^{3+}$  ions and the reverse energy transfer from  $\text{Sm}^{3+}$  to  $\text{Tb}^{3+}$  ions. Taking advantage of these energy transfer channels, the color coordinates of the material could be changed from yellowish-pink and yellowish-green emissions to white emission by controlling the ratio of ions doped in TNLC glasses. The optimal molar concentration ratio between  $\text{Tb}^{3+}$  and  $\text{Sm}^{3+}$  ions for the best white light emission was 0.83 for the TNLC-0.5Tb0.6Sm sample. Changing the ratio of these rare-earth (RE) ions allowed tuning the color temperature of the material from 5616 to 7699 K. Thus,  $\text{Tb}^{3+}$ – $\text{Sm}^{3+}$  co-doped and  $\text{Tb}^{3+}$ – $\text{Sm}^{3+}$ – $\text{Yb}^{3+}$  tri-doped TNLC glasses are promising materials for color display applications and white light-emitting diodes (WLEDs).

Received 15th April 2025  
 Accepted 4th May 2025

DOI: 10.1039/d5ra02624e  
[rsc.li/rsc-advances](http://rsc.li/rsc-advances)

## 1. Introduction

In recent years, with the rapid development and high demand of optoelectronic materials for color display technologies and devices,<sup>1,2</sup> light-emitting diodes (LEDs)<sup>3,4</sup> that emit in the visible region, display full colors and are color-tunable are in high demand, promoting extensive research on rare-earth (RE)-ion

doping in various host matrices,<sup>5–7</sup> such as phosphors, glasses, and glass-ceramic containing nanocrystals. Among various host matrices, tellurite-based glasses have emerged as promising candidates owing to their unique physicochemical and optical properties.<sup>5,6</sup> Tellurite-based glasses have a relatively low melting point, high thermal stability, good RE ion solubility, a wide transmission window (covering the visible (VIS) to near-infrared (NIR) region), and low phonon energy (which minimizes non-radiative (NR) losses and enhances emission efficiency).<sup>7,8</sup> Co-doping RE ions in tellurite glasses facilitates sharp, well-defined intra-4f electronic transitions that result in highly stable and efficient luminescence. The incorporation of RE ions in tellurite glasses further opens up pathways for energy transfer (ET) interactions, enabling the tuning of emission intensity and chromaticity of color in the visible wavelength range.<sup>9,10</sup> The combination of  $\text{Sm}^{3+}$ ,  $\text{Tb}^{3+}$ , and  $\text{Yb}^{3+}$  ions produces a cooperative, energy-transferring, and tunable emission intensity and colorimetry for visible and upconversion (UC) emissions when excited at different wavelengths.<sup>11</sup>  $\text{Sm}^{3+}$  ions exhibit prominent orange-red emission around 600–650 nm, corresponding to  ${}^4\text{G}_{5/2} \rightarrow {}^6\text{H}_{7/2}$  and  ${}^4\text{G}_{5/2} \rightarrow {}^6\text{H}_{5/2}$  transitions;<sup>12,13</sup>  $\text{Tb}^{3+}$  ions produce strong green emission near 546 nm, corresponding to  ${}^5\text{D}_4 \rightarrow {}^7\text{F}_5$  transition,<sup>14,15</sup> and  $\text{Yb}^{3+}$  ions exhibit only one  ${}^2\text{F}_{5/2} \rightarrow {}^2\text{F}_{7/2}$  transition and acts as a sensitizer owing to their strong absorption at  $\sim$ 980 nm and the ability to participate in UC and cross-relaxation (CR)

<sup>a</sup>Optical Materials Research Group, Science and Technology Advanced Institute, Van Lang University, Ho Chi Minh City, Vietnam. E-mail: [hokimdan@vlu.edu.vn](mailto:hokimdan@vlu.edu.vn)

<sup>b</sup>Faculty of Applied Technology, School of Technology, Van Lang University, Ho Chi Minh City, Vietnam

<sup>c</sup>Faculty of Chemistry and Environment, Dalat University, Lam Dong, Vietnam

<sup>d</sup>Faculty of Basic Sciences, University of Phan Thiet, 225 Nguyen Thong, Phan Thiet City, Binh Thuan, Vietnam

<sup>e</sup>Institute of Science and Technology, TNU-University of Sciences, Thai Nguyen 250000, Vietnam

<sup>f</sup>Institute of Theoretical and Applied Research, Duy Tan University, Hanoi 100000, Vietnam. E-mail: [vutkimlien@duytan.edu.vn](mailto:vutkimlien@duytan.edu.vn)

<sup>g</sup>Faculty of Natural Sciences, Duy Tan University, Da Nang 550000, Vietnam

<sup>h</sup>The University of Danang, University of Science and Education, Da Nang, 550000, Vietnam

<sup>i</sup>Faculty of Engineering and Technology, Nguyen Tat Thanh University, Ho Chi Minh City, Vietnam

<sup>j</sup>Key Laboratory of Advanced Materials of Yunnan Province, Kunming University of Science and Technology, Kunming 650093, China

† Electronic supplementary information (ESI) available. See DOI: <https://doi.org/10.1039/d5ra02624e>



mechanisms.<sup>16,17</sup> Some works have explored the color tunability, luminescence properties, and ET mechanisms in RE ion co-doped glasses/glass ceramics to develop materials suitable for color display and LED applications.<sup>18–20</sup> F. Nawaz *et al.*<sup>21</sup> investigated and reported the influence of Yb<sup>3+</sup> co-doping on the optical properties of Sm<sup>3+</sup>-doped sodium tellurite glasses. They found that Yb<sup>3+</sup> co-doping affected the absorption and emission characteristics of Sm<sup>3+</sup> ions, indicating ET between the Sm<sup>3+</sup> and Yb<sup>3+</sup> ions.<sup>21</sup> J. Li *et al.*<sup>22</sup> reported a multi-color afterglow in Tb<sup>3+</sup>-Sm<sup>3+</sup> co-doped gallo-silicate glass ceramics. By adjusting the concentrations of Tb<sup>3+</sup> and Sm<sup>3+</sup> ions, the afterglow emission could be tuned from green to orange and then to yellow.<sup>22</sup> This study highlighted ET and trap-sharing mechanisms between the dopants, which are significant for optical anti-counterfeiting applications. In general, these studies collectively enhance our understanding of ET dynamics and luminescence tuning in RE co-doped tellurite glass systems, contributing to the development of materials for color displays, LEDs, and other photonic applications.<sup>21,22</sup>

Lithium–niobium–tellurite (Li–Nb–Te) glass is particularly advantageous as a host because the incorporation of lithium and niobium oxides enhances the structural network,<sup>23</sup> improves RE ion dispersion, and increases the optical bandgap and nonlinear optical properties. The presence of Nb<sup>5+</sup> ions, which act as a glass modifier, can influence local field symmetry and aid the creation of non-centrosymmetric sites that are beneficial for RE ion emission.<sup>23,24</sup> Furthermore, the addition of Li<sub>2</sub>O serves to improve glass formability and optical clarity while also aiding ET dynamics by modifying the local coordination environment of the RE ions.<sup>25</sup> Although several studies have explored tellurite glasses single-doped and co-doped with Tb<sup>3+</sup>, Sm<sup>3+</sup>, and Yb<sup>3+</sup> ions, as well as other optical materials containing these RE ions, most of them have focused on ET mechanisms from Tb<sup>3+</sup> to Sm<sup>3+</sup> ions. However, reverse ET

mechanisms, such as from Sm<sup>3+</sup> to Tb<sup>3+</sup> ions or from Yb<sup>3+</sup> to both Tb<sup>3+</sup> and Sm<sup>3+</sup> ions, have not been reported. These mechanisms are crucial for enabling strong visible emission under 980 nm infrared excitation, corresponding to the transition of Yb<sup>3+</sup> from the <sup>2</sup>F<sub>7/2</sub> to <sup>2</sup>F<sub>5/2</sub> state. In this study, TeO<sub>2</sub>–Nb<sub>2</sub>O<sub>5</sub>–Li<sub>2</sub>O–CaO (TNLC) glasses with various doping schemes, including Tb<sup>3+</sup>-doped, Sm<sup>3+</sup>-doped, Tb<sup>3+</sup>–Sm<sup>3+</sup> co-doped, and Tb<sup>3+</sup>–Sm<sup>3+</sup>–Yb<sup>3+</sup> tri-doped glasses, were synthesized *via* melt-quenching. We investigated the effect of varying the concentrations of these ions on the emission color. A detailed analysis of the ET processes from Tb<sup>3+</sup> to Sm<sup>3+</sup>, Sm<sup>3+</sup> to Tb<sup>3+</sup>, and Yb<sup>3+</sup> to both Tb<sup>3+</sup> and Sm<sup>3+</sup> ions was conducted. By adjusting the ion ratios, white-light emission was achieved. These findings suggest that TNLC glasses co-doped with Tb<sup>3+</sup>, Sm<sup>3+</sup>, and Yb<sup>3+</sup> ions are promising candidates for color display technologies and white light-emitting diodes (LEDs).

## 2. Experimental details

The lithium–niobium–tellurite glasses used in this work were synthesized using a conventional melt-quenching technique. High-purity laboratory-grade reagents (99.99%), including TeO<sub>2</sub>, Nb<sub>2</sub>O<sub>5</sub>, Li<sub>2</sub>O, CaO, TbF<sub>3</sub>, Sm<sub>2</sub>O<sub>3</sub>, and Yb<sub>2</sub>O<sub>3</sub>, were used as raw materials. Specific compositions, molar ratios, and corresponding sample abbreviations are summarized in Table 1.

Approximately 12 grams of each glass batch was prepared by accurately weighing the required mixtures of raw materials using an electronic analytical balance. After finely grinding them using an onyx mortar and agate pestle, the mixtures were compacted, placed in a platinum crucible and then heated in a Nabertherm electric furnace (Germany) at 1150 °C for 45 minutes under an air atmosphere.<sup>16,26,27</sup> Following the melting process, the molten materials were cast into molds and rapidly cooled on a stainless-steel plate to form the initial glass

**Table 1** Specific glass compositions and molar concentration ratios of the as-synthesized TeO<sub>2</sub>–Nb<sub>2</sub>O<sub>5</sub>–Li<sub>2</sub>O–CaO–TbF<sub>3</sub>–Sm<sub>2</sub>O<sub>3</sub>–Yb<sub>2</sub>O<sub>3</sub> lithium–niobium–tellurite glasses

Glass sample	Molar concentration ratio of the components						
	TeO <sub>2</sub>	Nb <sub>2</sub> O <sub>5</sub>	Li <sub>2</sub> O	CaO	TbF <sub>3</sub>	Sm <sub>2</sub> O <sub>3</sub>	Yb <sub>2</sub> O <sub>3</sub>
TNLC-0.5Tb	60	18	12	9.5	0.5	0	0
TNLC-0.5Sm	60	18	12	9.5	0	0.5	0
TNLC-0.5Tb0.5Sm	60	18	12	9.0	0.5	0.5	0
TNLC-0.6Tb0.5Sm	60	18	12	8.9	0.6	0.5	0
TNLC-0.7Tb0.5Sm	60	18	12	8.8	0.7	0.5	0
TNLC-0.8Tb0.5Sm	60	18	12	8.7	0.8	0.5	0
TNLC-0.9Tb0.5Sm	60	18	12	8.6	0.9	0.5	0
TNLC-1.0Tb0.5Sm	60	18	12	8.5	1.0	0.5	0
TNLC-0.5Tb0.6Sm	60	18	12	8.9	0.5	0.6	0
TNLC-0.5Tb0.7Sm	60	18	12	8.8	0.5	0.7	0
TNLC-0.5Tb0.8Sm	60	18	12	8.7	0.5	0.8	0
TNLC-0.5Tb0.9Sm	60	18	12	8.6	0.5	0.9	0
TNLC-0.5Tb1.0Sm	60	18	12	8.5	0.5	1.0	0
TNLC-0.5Tb0.5Sm2Yb	60	18	12	7.0	0.5	0.5	2
TNLC-0.6Tb0.5Sm2Yb	60	18	12	6.9	0.6	0.5	2
TNLC-0.7Tb0.5Sm2Yb	60	18	12	6.8	0.7	0.5	2
TNLC-0.8Tb0.5Sm2Yb	60	18	12	6.7	0.8	0.5	2
TNLC-1.0Tb0.5Sm2Yb	60	18	12	6.5	1.0	0.5	2



samples. To enhance the mechanical strength and eliminate residual thermal stresses, the glass samples were annealed at approximately 342 °C for 10 hours.<sup>26,27</sup> The TNLC glass materials used for optical measurements were cut into samples with approximate dimensions of 10 mm × 10 mm × 2 mm. These TNLC glass samples were then thoroughly polished on the edges and surfaces. Differential thermal analysis (DTA) was performed on a Shimadzu DTG-60H TG/DTA. The absorption spectra of the TNLC glasses in the wavelength range of 350–2000 nm were recorded using a Hitachi U-4100 UV/VIS/NIR spectrophotometer. The excitation, visible, and UC emission spectra of the  $Tb^{3+}$ -doped,  $Sm^{3+}$ -doped,  $Tb^{3+}$ – $Sm^{3+}$  co-doped,  $Tb^{3+}$ – $Sm^{3+}$ – $Yb^{3+}$  tri-doped TNLC glasses were measured in the wavelength range of 200 to 750 nm using an Edinburgh Instruments FLS-1000 photoluminescence spectrometer. All the absorption, excitation, visible, and UC emission spectral measurements, and decay lifetime analyses of the TNLC glass samples were performed at ambient temperature.<sup>26,27</sup>

### 3. Results and discussion

DTA was conducted to investigate the thermal stability and glass-forming ability of the lithium–niobium–tellurite glass using the TNLC-0.5Tb0.5Sm2Yb glass sample. The DTA curve was recorded in the 100 to 1000 °C temperature range at a constant heating rate (typically 10 °C min<sup>-1</sup>) under a nitrogen atmosphere. The DTA curve revealed typical thermal parameters. The onset of endothermic deviation in the DTA curve corresponded with the glass transition temperature ( $T_g$ ), which was observed at approximately 342 °C. This  $T_g$  value indicates the temperature at which the amorphous glass matrix transitions from a rigid, glassy state to a more flexible, rubbery state. A relatively low  $T_g$  is characteristic of tellurite-based glasses and is attributed to the weak Te–O bonds and the open network structure of the tellurite matrix. An exothermic peak was observed at around 493 °C, corresponding to the onset of crystallization ( $T_x$ ). This temperature indicates the initiation of

structural reorganization and phase separation within the glass matrix, leading to the formation of crystalline phases.<sup>16,28,29</sup> The difference between  $T_x$  and  $T_g$  was  $\Delta T = T_x - T_g = (493 - 342)$  °C = 151 °C; often referred to as the thermal stability window, it is an important parameter to evaluate glass stability against devitrification.<sup>16,29,30</sup> For the TNLC-0.5Tb0.5Sm2Yb sample, the  $\Delta T$  of approximately 151 °C indicates reasonably good thermal stability and suggests that the material is suitable for optical applications that require thermal processing.<sup>16</sup> Besides, the values of crystallization temperature ( $T_c$ ) and crystallization peak temperatures  $T_p$  (including  $T_{p1}$ ,  $T_{p2}$ , and  $T_{p3}$  temperatures)<sup>16</sup> were also determined to be ~598, 637, 786, and 851 °C, respectively, as depicted in Fig. 1.

The absorption spectra of TNLC-0.5Tb, TNLC-0.5Sm, TNLC-0.5Tb0.5Sm, and TNLC-0.5Tb0.5Sm2Yb lithium–niobium–tellurite glass samples are shown in Fig. 2. The absorption spectra characterize the  $Tb^{3+}$  ions due to f–f transitions. These transitions typically occur in the ultraviolet (UV) and visible wavelength regions, primarily at ~398 and 480 nm, corresponding to the  $^7F_6 \rightarrow ^5D_3$  and  $^7F_6 \rightarrow ^5D_4$  transitions of  $Tb^{3+}$  ions.<sup>18,31</sup>  $Sm^{3+}$  has different absorption characteristics from  $Tb^{3+}$ , primarily because of the 4f states. The absorption peaks of  $Sm^{3+}$  are typically broader than those of the  $Tb^{3+}$  ions due to the nature of its electronic transitions. The absorption spectrum of  $Sm^{3+}$  in the wavelength range of 350–2000 nm includes peaks at ~360, 374, 402, 473, 939, 1076, 1224, 1369, 1472, and 1536 nm attributed to the  $^6H_{5/2} \rightarrow ^6P_{7/2}$ ,  $^6P_{7/2}$ ,  $^4F_{7/2}$ ,  $^4F_{11/2}$ ,  $^6F_{11/2}$ ,  $^6F_{9/2}$ ,  $^6F_{7/2}$ ,  $^6F_{5/2}$ ,  $^6F_{3/2}$  and  $^6H_{15/2}$  transitions, respectively.<sup>4,22,32</sup> The absorption spectrum of the  $Tb^{3+}$ – $Sm^{3+}$  co-doped TNLC-0.5Tb0.5Sm glass sample in the wavelength range of 350–2000 nm contains all the absorption peaks of  $Tb^{3+}$  and  $Sm^{3+}$  ions.<sup>4,22,32–34</sup> The absorption spectrum of the  $Tb^{3+}$ – $Sm^{3+}$ – $Yb^{3+}$  tri-doped TNLC-0.5Tb0.5Sm2Yb glass sample in the wavelength range of 350–2000 nm includes all the absorption peaks of  $Tb^{3+}$ ,  $Sm^{3+}$  ions and the absorption peak of  $Yb^{3+}$  ions at ~975 nm ( $^2F_{7/2} \rightarrow ^2F_{5/2}$ ).

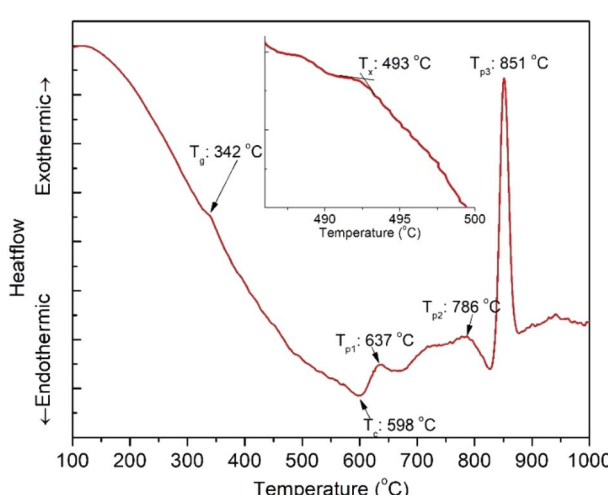


Fig. 1 DTA analysis of the TNLC-0.5Tb0.5Sm2Yb lithium–niobium–tellurite glass sample.

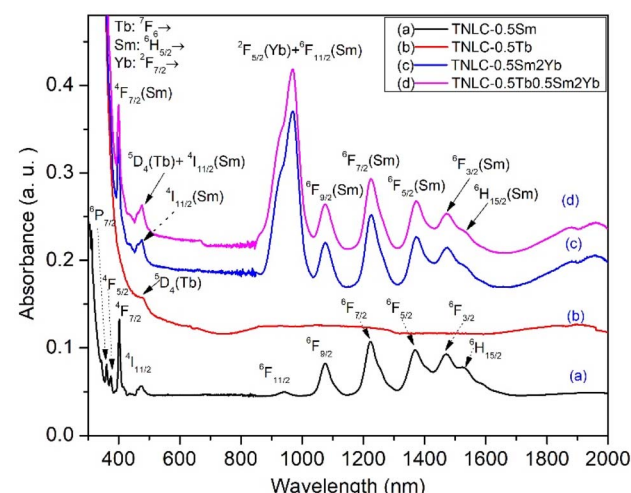


Fig. 2 Absorption spectra of TNLC-0.5Tb, TNLC-0.5Sm, TNLC-0.5Tb0.5Sm, and TNLC-0.5Tb0.5Sm2Yb lithium–niobium–tellurite glass samples.



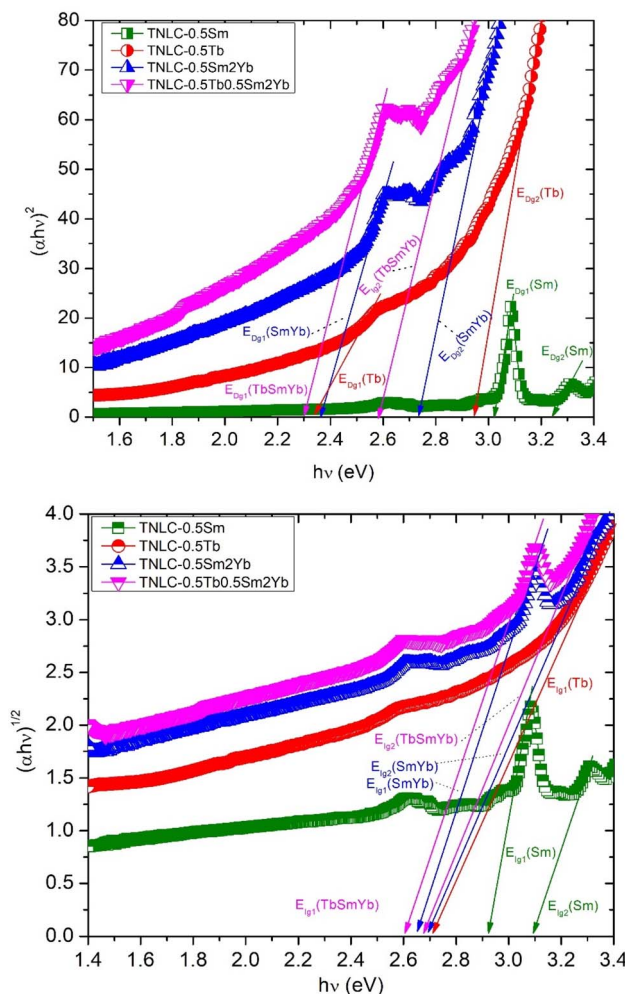


Fig. 3 (a) Direct optical bandgaps of the TNLC-0.5Sm, TNLC-0.5Tb, TNLC-0.5Sm2Yb, and TNLC-0.5Tb0.5Sm2Yb glass samples. (b) Indirect optical bandgaps of the TNLC-0.5Sm, TNLC-0.5Tb, TNLC-0.5Sm2Yb, and TNLC-0.5Tb0.5Sm2Yb glass samples.

The direct optical bandgaps (DOB) and indirect optical bandgaps (IOB) of the TNLC-0.5Sm, TNLC-0.5Tb, TNLC-0.5Sm2Yb, and TNLC-0.5Tb0.5Sm2Yb glass samples were calculated and analyzed based on their absorption spectra using the Tauc formula:<sup>19,35,36</sup>

$$\alpha(\lambda) = B \frac{(h\nu - E_g)^\gamma}{h\nu} \quad (1)$$

Here,  $\alpha(\lambda)$  is the absorption coefficient;  $\lambda$  is the wavelength;  $\nu$  is the frequency;  $h$  is the Planck constant;  $B$  is the energy-independent constant;<sup>19,35,36</sup>  $E_g$  is the energy gap of the glass samples;  $\gamma = 2$  for DOB;  $\gamma = \frac{1}{2}$  for IOB.<sup>19,35,36</sup> The calculated direct optical bandgaps (DOB) of the TNLC-0.5Sm, TNLC-0.5Tb, TNLC-0.5Sm2Yb, and TNLC-0.5Tb0.5Sm2Yb glass samples are shown in Fig. 3(a).

Similarly, the indirect optical bandgaps of the TNLC-0.5Sm, TNLC-0.5Tb, TNLC-0.5Sm2Yb, and TNLC-0.5Tb0.5Sm2Yb glass samples were calculated based on their absorption spectra using the Tauc formula, as shown in Fig. 3(b). A summary of the energy indirect/direct bandgap values of the TNLC-0.5Tb, TNLC-0.5Sm, TNLC-0.5Tb0.5Sm, and TNLC-0.5Tb0.5Sm2Yb glass samples is presented in Table 2.

As shown in Table 2, all the glass samples exhibited significantly smaller bandgaps than pure  $\text{TeO}_2$  glass. The incorporation of  $\text{Nb}_2\text{O}_5$ ,  $\text{CaO}$ , and  $\text{Li}_2\text{O}$  introduces electronic states within the  $\text{TeO}_2$  bandgap, resulting in a notable reduction in the band gap. Among the samples, the TNLC-0.5Sm glass sample had a larger bandgap than the TNLC-0.5Tb glass sample, though both remain smaller than that of pure  $\text{TeO}_2$ . This reduction is attributed to the addition of RE ions, which alter the glass network by modifying oxygen bonding, increasing non-bridging oxygen content, and affecting light absorption. Furthermore, the TNLC-0.5Sm2Yb and TNLC-0.5Tb0.5Sm2Yb glass samples showed even lower bandgaps owing to the higher RE ion concentrations, which introduced additional intermediate energy levels and further enhanced non-bridging oxygen states. The increasing concentration of RE ions in the glass matrix also increases the non-bridging oxygen bonding state, causing the band gap of the glass to decrease.

The excitation spectra of the TNLC-0.5Tb, TNLC-0.5Sm, and TNLC-0.5Tb0.5Sm glass samples were obtained, as shown in Fig. 4, to determine the excitation wavelengths for the TNLC glass samples containing both  $\text{Tb}^{3+}$  and  $\text{Sm}^{3+}$  ions. Based on the spectral data, we chose 374 nm as the excitation wavelength for the  $\text{Tb}^{3+}$ - $\text{Sm}^{3+}$  co-doped TNLC glass sample.<sup>37,38</sup>

The visible emission spectra of the TNLC-0.5Tb, TNLC-0.5Sm, and TNLC-0.5Tb0.5Sm lithium-niobium-tellurite glass samples under 374 nm are shown in Fig. 5. For the TNLC-0.5Tb glass sample, the visible emission of  $\text{Tb}^{3+}$  under 374 nm excitation revealed weaker peaks at around 415 and 438 nm due to the  $^3\text{D}_5 \rightarrow ^7\text{F}_5$  and  $^3\text{D}_5 \rightarrow ^7\text{F}_4$  transitions.<sup>4,16,32</sup> This result is intriguing because these emission peaks have not been reported in most previous works. For the TNLC-0.5Sm glass sample, the

Table 2 Indirect/direct energy bandgap values of the TNLC-0.5Tb, TNLC-0.5Sm, TNLC-0.5Tb0.5Sm, and TNLC-0.5Tb0.5Sm2Yb glass samples

Glass sample	Direct bandgap values			Indirect bandgap values		
	$E_{Dg1}$ (eV)	$E_{Dg2}$ (eV)	$\Delta E_D = E_{Dg2} - E_{Dg1}$ (eV)	$E_{Ig1}$ (eV)	$E_{Ig2}$ (eV)	$\Delta E_I = E_{Ig2} - E_{Ig1}$ (eV)
TNLC-0.5Sm	3.02	3.23	0.21	2.98	3.19	0.21
TNLC-0.5Tb	2.34	2.95	0.61	2.84	—	—
TNLC-0.5Sm2Yb	2.36	2.74	0.38	2.75	2.82	0.07
TNLC-0.5Tb0.5Sm2Yb	2.28	2.59	0.31	2.72	2.79	0.07



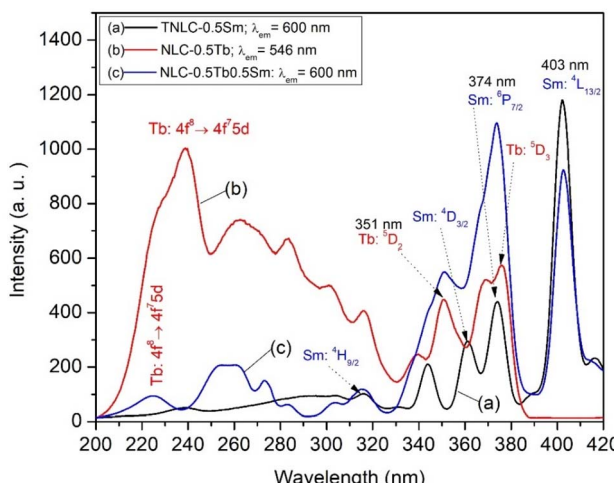


Fig. 4 Excitation spectra of the TNLC-0.5Tb, TNLC-0.5Sm, and TNLC-0.5Tb0.5Sm lithium-niobium-tellurite glass samples.

visible emission peaks of  $\text{Sm}^{3+}$  under 374 nm excitation at around 440, 564, 601, and 645 nm could be attributed to the  ${}^4\text{G}_{7/2} \rightarrow {}^6\text{H}_{9/2}$ ,  ${}^4\text{G}_{5/2} \rightarrow {}^6\text{H}_{5/2}$ ,  ${}^4\text{G}_{5/2} \rightarrow {}^6\text{H}_{7/2}$ , and  ${}^4\text{G}_{5/2} \rightarrow {}^6\text{H}_{9/2}$  transitions, respectively.<sup>32–34</sup> For the TNLC-0.5Tb0.5Sm glass sample, the visible emission of peaks co-doped  $\text{Tb}^{3+}$  and  $\text{Sm}^{3+}$  under 374 nm excitation were found at around 415, 438, 490, 546, 587, 622, and 645 nm due to transitions from  $\text{Tb}^{3+}$ ,  $\text{Sm}^{3+}$  ions or the combination of transitions from both  $\text{Tb}^{3+}$  and  $\text{Sm}^{3+}$  ions corresponding to ( $\text{Tb}^{3+}$ :  ${}^3\text{D}_5 \rightarrow {}^7\text{F}_5$ ), ( $\text{Tb}^{3+}$ :  ${}^3\text{D}_5 \rightarrow {}^7\text{F}_4$  +  $\text{Sm}^{3+}$ :  ${}^4\text{G}_{7/2} \rightarrow {}^6\text{H}_{9/2}$ ), ( $\text{Tb}^{3+}$ :  ${}^3\text{D}_4 \rightarrow {}^7\text{F}_{J=6, 5, 4, \text{ and } 3}$ ) and ( $\text{Sm}^{3+}$ :  ${}^4\text{G}_{5/2} \rightarrow {}^6\text{H}_{9/2}$ ) transitions, respectively.<sup>4,32–34</sup>

The Commission Internationale de L'Eclairage (CIE) 1931 ( $x$ ;  $y$ ) chromaticity coordinates<sup>19,39</sup> for the visible emission spectra of the TNLC-0.5Tb, TNLC-0.5Sm, and TNLC-0.5Tb0.5Sm glass samples were determined to be  $P_{\text{Tb}}$  (0.2840; 0.5303),  $P_{\text{Sm}}$  (0.2901; 0.3728), and  $P_{\text{Sm}}$  (0.4906; 0.3537) located in the

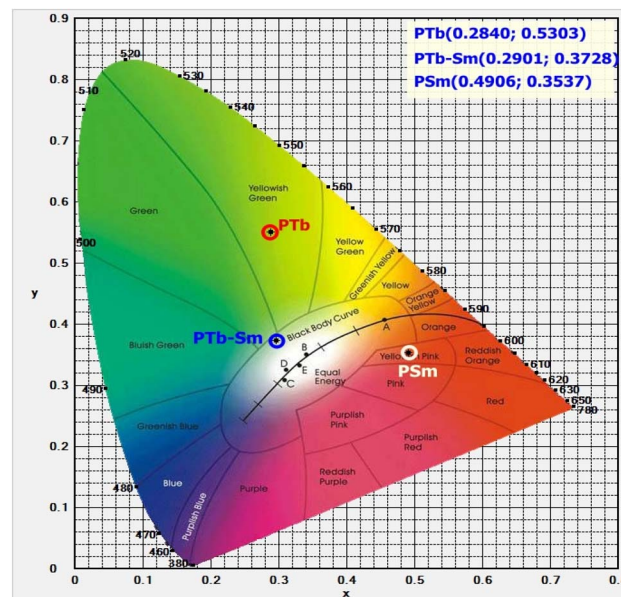


Fig. 6 CIE 1931 ( $x$ ;  $y$ ) color coordinates for the visible emission spectra of the TNLC-0.5Tb, TNLC-0.5Sm, and TNLC-0.5Tb0.5Sm glass samples under 374 nm excitation.

yellow-pink, yellowish-green and black body curve regions, respectively, as shown in Fig. 6.

The visible emission spectra of the TNLC- $p$ Tb0.5Sm ( $p$  = 0.6, 0.7, 0.8, 0.9, and 1.0 mol%) lithium-niobium-tellurite glass samples under 374 nm are shown in Fig. 7. With the increase in molar concentration of  $\text{Tb}^{3+}$  from 0.6 to 1.0 mol%, the visible emission intensity of the peaks of  $\text{Tb}^{3+}$  ions at ~415, 438, 490, 546, and 622 nm increased significantly.<sup>32,33</sup> Similarly, the visible emission intensity of the  $\text{Sm}^{3+}$  ion peaks at around 645 nm, which is attributed to the  ${}^4\text{G}_{5/2} \rightarrow {}^6\text{H}_{9/2}$  transition, was also increased. These findings confirm that energy from the neighboring states of  $\text{Tb}^{3+}$  ions were transferred to the  ${}^4\text{G}_{5/2} \rightarrow {}^6\text{H}_{9/2}$  transition of  $\text{Sm}^{3+}$  ions.<sup>33,34,37–40</sup>

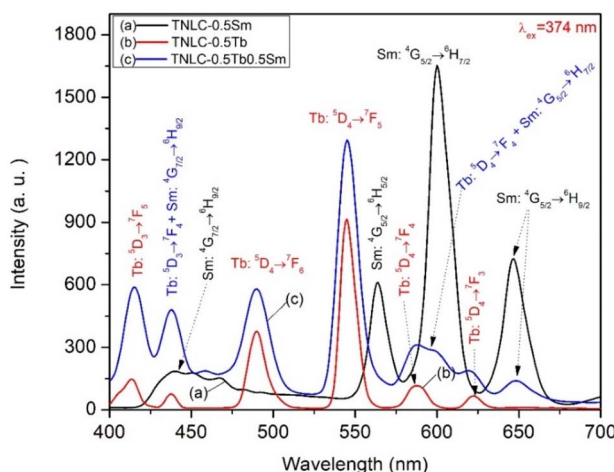


Fig. 5 Visible emission spectra of the TNLC-0.5Tb, TNLC-0.5Sm, and TNLC-0.5Tb0.5Sm lithium-niobium-tellurite glass samples under 374 nm excitation.

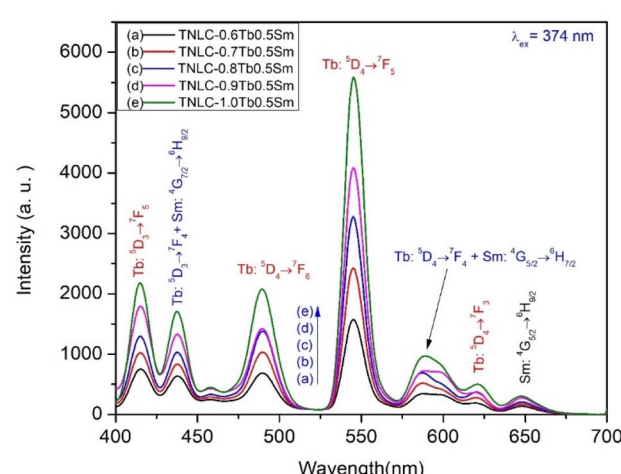
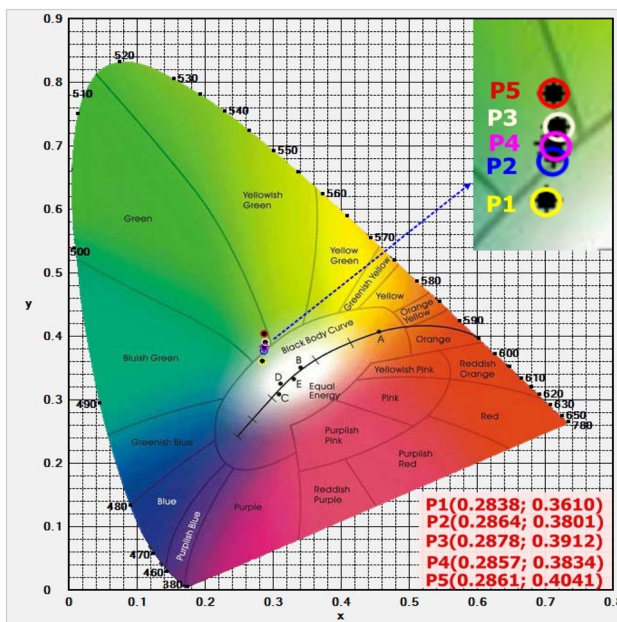


Fig. 7 Visible emission spectra of the TNLC- $p$ Tb0.5Sm ( $p$  = 0.6, 0.7, 0.8, 0.9, and 1.0 mol%) glass samples under 374 nm excitation.





**Fig. 8** CIE 1931 ( $x$ ;  $y$ ) color coordinates for the visible emission spectra of the TNLC- $p$ Tb0.5Sm ( $p = 0.6, 0.7, 0.8, 0.9$ , and  $1.0$  mol%) glass samples under 374 nm excitation.

Fig. 8 shows the CIE1931 ( $x$ ;  $y$ ) color coordinates for the visible emission spectra of the TNLC- $p$ Tb0.5Sm ( $p$  = 0.6, 0.7, 0.8, 0.9, and 1.0 mol%) lithium-niobium-tellurite glass samples under excitation at 374 nm. With the increase in the molar concentration of  $\text{Tb}^{3+}$  ions from 0.6 to 1.0 mol%, the color points of the visible emission spectra of the  $\text{Tb}^{3+}$ - $\text{Sm}^{3+}$  co-doped glass shifted in the order of P1 (0.2838; 0.3610), P2 (0.2864; 0.3801), P3 (0.2878; 0.3912), P4 (0.2857; 0.3834) and P5 (0.2861; 0.4041) in the CIE1931 ( $x$ ;  $y$ ) color coordinate chart, respectively,<sup>19,33,34</sup> as shown in Fig. 8. From the results in Fig. 8, we can see that the TNLC-0.6Tb0.5Sm sample corresponding to the  $\text{Tb}^{3+}/\text{Sm}^{3+}$  concentration ratio of 1.2 has the color point closest to the white light region.<sup>33,34</sup>

To further investigate the optimal concentration ratio between  $Tb^{3+}$  and  $Sm^{3+}$  ions for the color point to move closer to the white light region, which is necessary for application to WLEDs, the  $Sm^{3+}$  concentration was changed while keeping the  $Tb^{3+}$  concentration constant to investigate the emission of the  $Tb^{3+}$ - $Sm^{3+}$  co-doped glass sample. The visible emission spectra of the TNLC-0.5TbqSm ( $q = 0.6, 0.7, 0.8, 0.9$ , and  $1.0\text{ mol\%}$ ) lithium-niobium-tellurite glass samples under 374 nm are shown in Fig. 9.

When excited at 374 nm, with an increase in  $\text{Sm}^{3+}$  concentration from 0.6 to 1.0 mol%, most of the emission peaks of both  $\text{Sm}^{3+}$  and  $\text{Tb}^{3+}$  ions increased in intensity. This result affirms that energy from the neighboring states of  $\text{Sm}^{3+}$  ions is transferred to the  $\text{Tb}^{3+}$  ions. Simultaneously, with the increase in molar concentration of  $\text{Sm}^{3+}$  ions from 0.6 to 1.0 mol%, the tunable color for the visible emission spectra of the  $\text{Tb}^{3+}$ – $\text{Sm}^{3+}$  co-doped glass samples shifted to color points 1 (0.3118; 0.3821), 2 (0.3093; 0.3827), 3 (0.3095; 0.3875), 4 (0.3169; 0.3937) and 5 (0.3263; 0.4049) on the CIE 1931 ( $x$ ;  $y$ ) coordinate

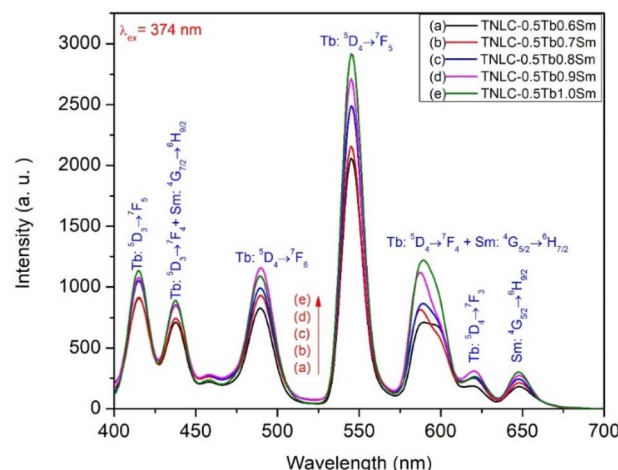


**Fig. 9** Visible emission spectra of the TNLC-0.5Tb<sub>2</sub>Sm (q = 0.6, 0.7, 0.8, 0.9, and 1.0 mol%) glass samples under 374 nm excitation

diagram,<sup>19,33,34</sup> as shown in Fig. 10. From the visible emission spectra results of the  $\text{Tb}^{3+}$ - $\text{Sm}^{3+}$  co-doped glass samples under 374 nm excitation (Fig. 7 and 9), as well as the color coordinates for their visible emission spectra (Fig. 8 and 10), we determined the optimal concentration ratio of  $\text{Tb}^{3+}$  and  $\text{Sm}^{3+}$  ions to be 0.83 for the color point to move the closest to the white light region, corresponding to the TNLC-0.5Tb0.6Sm glass sample.

During the analysis of the absorption capacity of the materials in the infrared region, we observed that the material strongly absorbed in the range from 940 to 1070 nm, with a maximum peak at about 980 nm. We surveyed the UC emission process of the  $\text{Tb}^{3+}$ - $\text{Sm}^{3+}$ - $\text{Yb}^{3+}$  co-doped material samples to investigate the ET process between  $\text{Yb}^{3+}$  ions and  $\text{Tb}^{3+}$ / $\text{Sm}^{3+}$

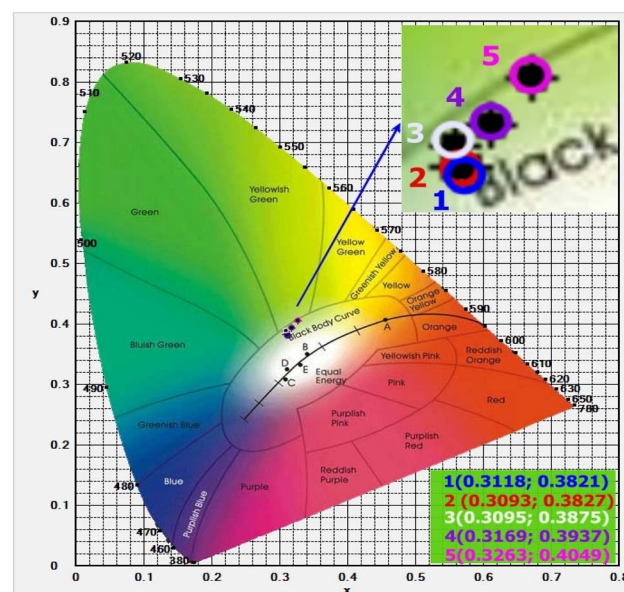


**Fig. 10** CIE1931 ( $x$ ;  $y$ ) color coordinates for the visible emission spectra of the TNLC-0.5Tb<sub>2</sub>Sm ( $q = 0.6, 0.7, 0.8, 0.9$ , and  $1.0$  mol%) glass samples under 374 nm excitation.

ions. In addition to investigating the VIS emission spectra of  $\text{Tb}^{3+}$ – $\text{Sm}^{3+}$  co-doped glass samples, we conducted further investigations using the UC emission spectra of these samples. Fig. 11 shows the UC emission spectra of the TNLC-*p*Tb0.5Sm2Yb (*p* = 0.5, 0.6, 0.7, 0.8, and 1.0 mol%) lithium-niobium-tellurite glass samples under a 980 nm laser diode (LD). With the increase in molar concentration of  $\text{Tb}^{3+}$  from 0.5 to 1.0 mol%, the UC emission intensity of the  $\text{Tb}^{3+}$  ion peaks at around 415, 438, 490, 546, and 622 nm increased for the  $\text{Tb}^{3+}$ – $\text{Sm}^{3+}$ – $\text{Yb}^{3+}$  co-doped glass samples.<sup>41</sup> Meanwhile, the UC emission intensity of the peaks at around 645 nm, attributed to the  ${}^4\text{G}_{5/2} \rightarrow {}^6\text{H}_{9/2}$  transition of  $\text{Sm}^{3+}$  ions, was also increased. This result confirms that energy from the neighboring states of  $\text{Tb}^{3+}$  ions was transferred to the  ${}^4\text{G}_{5/2} \rightarrow {}^6\text{H}_{9/2}$  transition of  $\text{Sm}^{3+}$  ions.<sup>39,40</sup>

Fig. 12 shows the CIE 1931 (*x*; *y*) color coordinates for the UC emission spectra of the TNLC-*p*Tb0.5Sm (*p* = 0.5, 0.6, 0.7, 0.8, and 1.0 mol%) lithium-niobium-tellurite glass samples under a 980 nm LD. With the increase in molar concentration of  $\text{Tb}^{3+}$  ions from 0.5 to 1.0 mol%, the color points shifted from in the order of points A (0.3277; 0.4847), B (0.2974; 0.5169), C (0.2997; 0.5441), D (0.3050; 0.5676), and E (0.3167; 0.5782) on the CIE 1931 (*x*; *y*) color coordinate diagram and were mainly located in the yellowish-green region.

To further determine the roles of excitation wavelength and the molar concentration of the doped RE ions on the CIE 1931 (*x*; *y*) color coordinates and color region, we compared the results obtained in this study with previously published reports, as listed in Table 3.

Investigation and calculation of correlated color temperature (CCT) are essential for optimizing the output light quality. From the CIE 1931 (*x*; *y*) results, the CCT of the TNLC glass samples was calculated using the McCamy formula (often called McCamy's approximation):<sup>50,52</sup>

$$\text{CCT} = an^3 + bn^2 + cn + d \approx -449n^3 + 3525n^2 - 6823.3n + 5520.33 \quad (3)$$

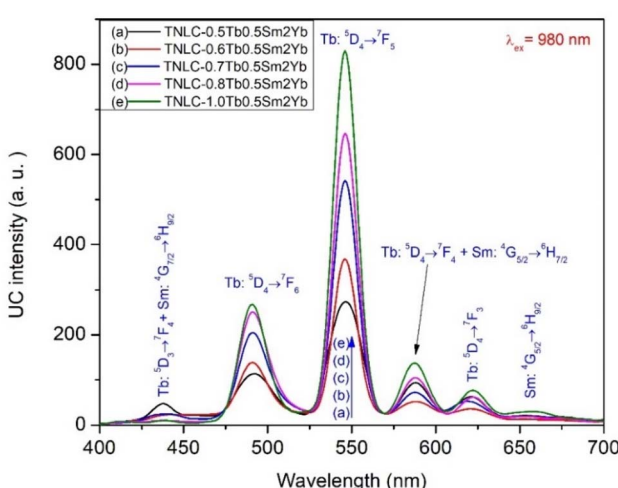


Fig. 11 UC emission spectra of the TNLC-*p*Tb0.5Sm2Yb (*p* = 0.5, 0.6, 0.7, 0.8, and 1.0 mol%) glass samples under 980 nm LD excitation.

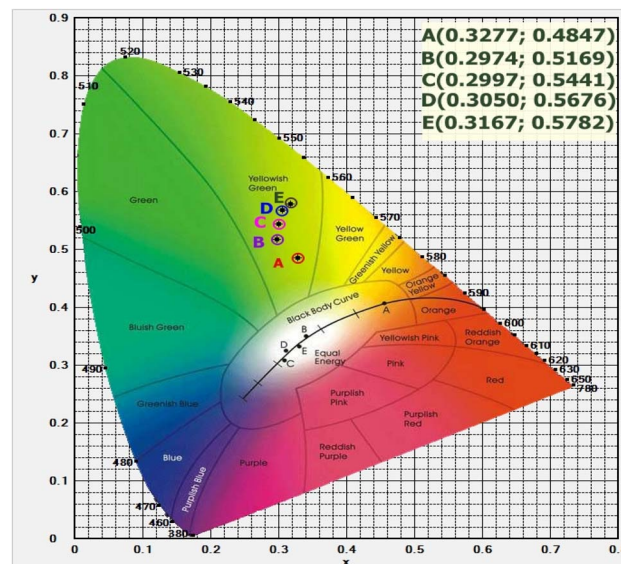


Fig. 12 CIE 1931 (*x*; *y*) color coordinates for the UC emission spectra of the TNLC-*p*Tb0.5Sm2Yb (*p* = 0.5, 0.6, 0.7, 0.8, and 1.0 mol%) glass samples excited under a 980 nm LD.

where:

$$n = \frac{x - x_e}{y - y_e}, \quad (4)$$

Here, *x* and *y* are the CIE 1931 (*x*; *y*) chromaticity coordinates of the light source;  $x_e = 0.3320$  and  $y_e = 0.1858$  are the chromaticity coordinates of the Planckian locus.<sup>50,52</sup> The CCT calculation results of the as-prepared glass samples are described in detail in Table 4.

The energy level diagram of the visible and UC emissions corresponding to the transitions of the  $\text{Tb}^{3+}$ – $\text{Sm}^{3+}$  and  $\text{Tb}^{3+}$ – $\text{Sm}^{3+}$ – $\text{Yb}^{3+}$  co-doped glass materials under excitation wavelengths of 374 nm and 980 nm is shown in Fig. 13. The  $\text{Tb}^{3+}$  ions are excited from the ground state  ${}^3\text{H}_6$  to the higher-energy state  ${}^3\text{D}_5$ . These ions show characteristic emission in the visible region due to  ${}^3\text{D}_5$  and  ${}^4\text{F}_4 \rightarrow {}^5\text{F}_J$  ( $J = 3, 4, 5$ , and  $6$ ) transitions.<sup>39</sup> Under 374 nm excitation, the visible emission of  $\text{Tb}^{3+}$  peaks at around 490, 546, 587, and 622 nm, which can be attributed to the  ${}^3\text{D}_4 \rightarrow {}^5\text{F}_J$  ( $J = 6, 5, 4$ , and  $3$ ) transitions. The  $\text{Sm}^{3+}$  ions, when excited at 374 nm, move from the  ${}^6\text{H}_{5/2}$  ground state to a higher-energy  ${}^6\text{P}_{7/2}$  state.<sup>40</sup> From this  ${}^6\text{P}_{7/2}$  state, energy is transferred to  ${}^4\text{G}_{5/2}$  lower-energy states through non-radiative and ET processes. The ET1, ET2, CET1, and CET2 processes shown in Fig. 13 can be described in detail as follows:<sup>41,51,53</sup>

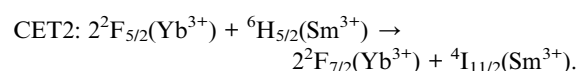
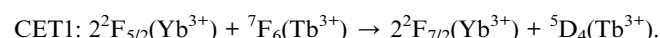
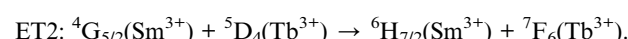
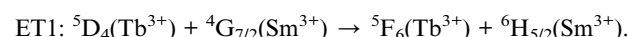
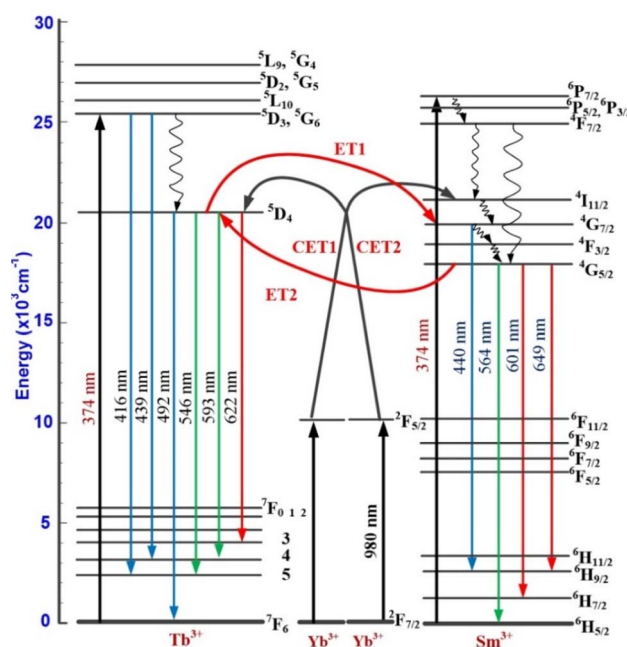


Table 3 Compare the energy transfer processes, color coordinates, and excitation wavelengths of RE ions in this study with those reported in previously published papers

Host material	RE co-doping ratio	$\lambda_{\text{ex}}$ (nm)	Energy transfer	CIE 1931 coordinates ( $x, y$ )	Color region	References
Tellurite glass	1Ce <sup>3+</sup> -1Tb <sup>3+</sup> -1Sm <sup>3+</sup>	350	Ce <sup>3+</sup> $\rightarrow$ Tb <sup>3+</sup>	0.3750; 0.3245	Pure white	T. T. Hong <i>et al.</i> <sup>42</sup>
Li <sub>2</sub> T <sub>4</sub> single crystals	1.24Tb <sup>3+</sup> -1.63Sm <sup>3+</sup> -0.25Ce <sup>3+</sup>	374	—	0.3084; 0.3612	Yellowish-green	Y. Z. Jiang <i>et al.</i> <sup>43</sup>
Ba <sub>3</sub> MgSi <sub>2</sub> O <sub>8</sub> :phosphors	0.12Tb <sup>3+</sup> -0.05Sm <sup>3+</sup>	233	Tb <sup>3+</sup> $\rightarrow$ Sm <sup>3+</sup>	0.555; 0.425	Orange yellow	X. K. Sun <i>et al.</i> <sup>44</sup>
Phosphate glasses	0.5Sm <sup>3+</sup> -0.1Tb <sup>3+</sup>	374	Tb <sup>3+</sup> $\rightarrow$ Sm <sup>3+</sup>	0.541; 0.300	Reddish-orange	K. A. Kumar <i>et al.</i> <sup>37</sup>
Zinc phosphate glasses	1.0Sm <sup>3+</sup> -0.1Tb <sup>3+</sup>	361	Tb <sup>3+</sup> $\rightarrow$ Sm <sup>3+</sup>	0.551; 0.312	Greenish-yellow	A. N. Meza-Rocha <i>et al.</i> <sup>45</sup>
	0.5Sm <sup>3+</sup> -1.0Tb <sup>3+</sup>	374	—	0.448; 0.459	Yellow	N. F. Andrade Neto <i>et al.</i> <sup>46</sup>
CaWO <sub>4</sub> nanoparticles	0.5Sm <sup>3+</sup> -0.5Tb <sup>3+</sup>	355	—	0.407; 0.485	White	K. Nie <i>et al.</i> <sup>47</sup>
	1.0Sm <sup>3+</sup> -1.0Tb <sup>3+</sup>	355	—	0.3098; 0.4033	Blue	N. F. Andrade Neto <i>et al.</i> <sup>48</sup>
Ca <sub>2</sub> La <sub>3</sub> (SiO <sub>4</sub> ) <sub>3</sub> F phosphor	0.15Tb <sup>3+</sup> , 0.04Sm <sup>3+</sup>	377	Tb <sup>3+</sup> $\rightarrow$ Sm <sup>3+</sup>	0.4175; 0.5658	Yellow-green	B. Yuan <i>et al.</i> <sup>49</sup>
	0.15Tb <sup>3+</sup> -0.18Sm <sup>3+</sup>	377	—	0.4691; 0.5160	Greenish-yellow	Y. N. Guo <i>et al.</i> <sup>50</sup>
CaLa <sub>4</sub> (SiO <sub>4</sub> ) <sub>3</sub> O <sub>2</sub> phosphors	9%Tb <sup>3+</sup> -11%Sm <sup>3+</sup>	377	Tb <sup>3+</sup> $\rightarrow$ Sm <sup>3+</sup>	0.393; 0.387	Bright white	
K <sub>3</sub> Gd(PO <sub>4</sub> ) <sub>2</sub> crystalline glass ceramics	0.3%Tb <sup>3+</sup> -0.4%Sm <sup>3+</sup>	376	Tb <sup>3+</sup> $\rightarrow$ Sm <sup>3+</sup>	0.3201; 0.3297	White	
K <sub>2</sub> Y(WO <sub>4</sub> ) <sub>2</sub> phosphors	2%Sm <sup>3+</sup> -5%Tb <sup>3+</sup>	377	Sm <sup>3+</sup> $\rightarrow$ Tb <sup>3+</sup>	0.37; 0.57	Yellow-green	E. J. Ansari <i>et al.</i> <sup>50</sup>
Potassium-zinc phosphate glasses	1.0Sm <sup>3+</sup> -1.0Tb <sup>3+</sup>	344	Tb <sup>3+</sup> $\rightarrow$ Sm <sup>3+</sup>	0.529; 0.447	Orange	O. Soriano-Romero <i>et al.</i> <sup>51</sup>
	1.0Sm <sup>3+</sup> -1.0Tb <sup>3+</sup>	360	Tb <sup>3+</sup> $\rightarrow$ Sm <sup>3+</sup>	0.534; 0.442	Yellow	
Lithium-niobium-tellurite glass	1.0Sm <sup>3+</sup> -1.0Tb <sup>3+</sup>	377	Tb <sup>3+</sup> $\rightarrow$ Sm <sup>3+</sup>	0.442; 0.507	Yellow	
	0.5Tb <sup>3+</sup> -0.6Sm <sup>3+</sup>	374	Tb <sup>3+</sup> $\leftrightarrow$ Sm <sup>3+</sup>	0.3118; 0.3821	White	
	0.5Tb <sup>3+</sup> -0.5Sm <sup>3+</sup> -2Yb <sup>3+</sup>	980	Yb <sup>3+</sup> $\rightarrow$ Tb <sup>3+</sup>	0.3277; 0.4847	(near black body curve)	
			Yb <sup>3+</sup> $\rightarrow$ Sm <sup>3+</sup>		Yellowish-green	

Table 4 CCT values and CIE 1931 ( $x$ ;  $y$ ) chromaticity coordinates of the TNLC glass samples

Glass samples	$\lambda_{\text{ex}}$	Color point	CIE 1931 $x$	CIE 1931 $y$	CCT (K)	Color region
TNLC-0.5Tb	374 nm	P <sub>Tb</sub>	0.2840	0.5303	6544	Yellowish green
TNLC-0.5Tb0.5Sm	374 nm	P <sub>Tb-Sm</sub>	0.2901	0.3728	7208	White
TNLC-0.5Sm	374 nm	P <sub>Sm</sub>	0.4906	0.3537	15 489	Yellowish pink
TNLC-0.6Tb0.5Sm	374 nm	P1	0.2838	0.3601	7662	Green
TNLC-0.7Tb0.5Sm	374 nm	P2	0.2864	0.3801	7294	Green
TNLC-0.8Tb0.5Sm	374 nm	P3	0.2878	0.3912	7129	Green
TNLC-0.9Tb0.5Sm	374 nm	P4	0.2857	0.3834	7290	Green
TNLC-1.0Tb0.5Sm	374 nm	P5	0.2861	0.4041	7085	Green
TNLC-0.5Tb0.6Sm	374 nm	1	0.3118	0.3821	6254	White
TNLC-0.5Tb0.7Sm	374 nm	2	0.3093	0.3827	6347	White
TNLC-0.5Tb0.8Sm	374 nm	3	0.3095	0.3875	6318	White
TNLC-0.5Tb0.9Sm	374 nm	4	0.3169	0.3937	6033	White
TNLC-0.5Tb1.0Sm	374 nm	5	0.3263	0.4049	5706	White
TNLC-0.5Tb0.5Sm2Yb	980 nm	A	0.3277	0.4847	5616	Yellowish green
TNLC-0.6Tb0.5Sm2Yb	980 nm	B	0.2974	0.5169	6274	Yellowish green
TNLC-0.7Tb0.5Sm2Yb	980 nm	C	0.2997	0.5441	6165	Yellowish green
TNLC-0.8Tb0.5Sm2Yb	980 nm	D	0.3050	0.5676	6020	Yellow
TNLC-1.0Tb0.5Sm2Yb	980 nm	E	0.3167	0.5782	5790	Yellowish green

Fig. 13 Energy levels of the  $\text{Tb}^{3+}$ ,  $\text{Sm}^{3+}$ , and  $\text{Yb}^{3+}$  ions and the mechanisms of visible and UC emissions via CET1, CET2, ET1, and ET2 processes in the TNLC glass system.

The charge transfer process between the  $\text{Tb}^{3+}$  and  $\text{Sm}^{3+}$  ions depends on the concentration of optical centers in the material. To further investigate the influence of  $\text{Tb}^{3+}$  ion concentration on the ET process, we analyzed the decay lifetimes of  $\text{Tb}^{3+}$  and  $\text{Sm}^{3+}$  ions in the synthesized TNLC glass materials. We measured the time-resolved fluorescence spectra of TNLC-0.5Tb $q$ Sm ( $q = 0, 0.6, 0.7, 0.8, 0.9$ , and  $1.0$  mol%) lithium-niobium-tellurite glass samples using an excitation wavelength of  $374$  nm and emission at  $546$  nm corresponding to the  ${}^5\text{D}_4 \rightarrow {}^5\text{F}_6$  transition of  $\text{Tb}^{3+}$ ;<sup>4,32-34</sup> the obtained results are presented in

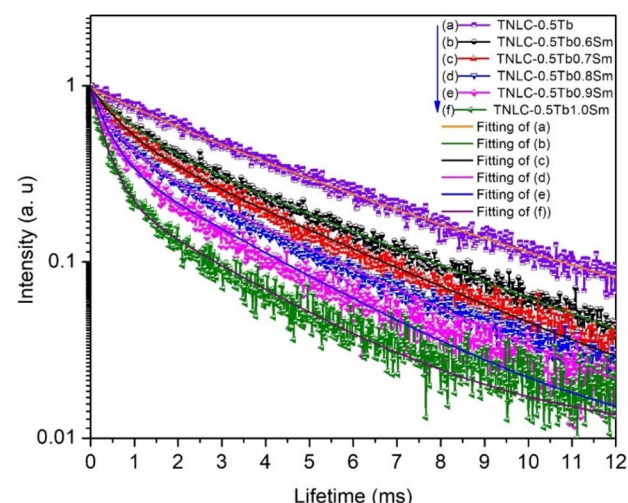
Fig. 14 Decay lifetimes of  $\text{Tb}^{3+}$  at the  ${}^5\text{D}_4 \rightarrow {}^5\text{F}_6$  transition in TNLC-0.5Tb $q$ Sm ( $q = 0, 0.6, 0.7, 0.8, 0.9$ , and  $1.0$  mol%) glass samples under  $374$  nm excitation.

Fig. 14. Through the fitting process, we observed that the time-resolved fluorescence spectra of the materials followed the equation:<sup>16,50</sup>

$$I_t = A_1 \exp\left(-\frac{t}{\tau_1}\right) + A_2 \exp\left(-\frac{t}{\tau_2}\right), \quad (5)$$

where  $\tau_1$  and  $\tau_2$  are the decay lifetime components, and  $A_1$  and  $A_2$  are constants. The average decay lifetime  $\tau$  was calculated as follows:<sup>16,51,54,55</sup>

$$\tau = \frac{A_1 \tau_1^2 + A_2 \tau_2^2}{A_1 \tau_1 + A_2 \tau_2}. \quad (6)$$

The decay lifetimes of TNLC-0.5Tb $q$ Sm ( $q = 0, 0.6, 0.7, 0.8, 0.9$ , and  $1.0$  mol%) lithium-niobium-tellurite glass samples



**Table 5** Decay lifetimes of  $\text{Tb}^{3+}$  ions at 546 nm ( $^5\text{D}_4 \rightarrow ^5\text{F}_6$ ) and  $\text{Sm}^{3+}$  ions at 564 nm ( $^4\text{G}_{5/2} \rightarrow ^6\text{H}_{5/2}$ ) under 374 nm excitation

Glass sample	Decay lifetime (ms)
TNLC-0.5Tb	4.62
TNLC-0.5Tb0.6Sm	3.97
TNLC-0.5Tb0.7Sm	3.48
TNLC-0.5Tb0.8Sm	3.13
TNLC-0.5Tb0.9Sm	2.63
TNLC-0.5Tb1.0Sm	2.21
TNLC-0.5Sm	7.86
TNLC-0.6Tb0.5Sm	6.91
TNLC-0.7Tb0.5Sm	5.63
TNLC-0.8Tb0.5Sm	4.24
TNLC-0.9Tb0.5Sm	3.18
TNLC-1.0Tb0.5Sm	2.56

calculated according to formula (6) are listed in Table 5. The decay lifetimes at 546 nm, corresponding to the  $^5\text{D}_4 \rightarrow ^5\text{F}_6$  transition of  $\text{Tb}^{3+}$  ions in the TNLC-0.5Tb $q$ Sm ( $q = 0, 0.6, 0.7, 0.8, 0.9$ , and  $1.0$  mol%) lithium-niobium-tellurite glass samples, were found to decrease with increasing  $\text{Sm}^{3+}$  concentration. This is strong evidence for ET from  $\text{Tb}^{3+}$  to  $\text{Sm}^{3+}$  ions.<sup>4,32–34,44</sup> Similarly, the decay lifetimes of  $\text{Sm}^{3+}$  ions at 601 nm, corresponding to the  $^4\text{G}_{5/2} \rightarrow ^6\text{H}_{7/2}$  transition of  $\text{Sm}^{3+}$  ions<sup>4,32–34</sup> in the TNLC- $p$ Tb0.5Sm ( $p = 0, 0.6, 0.7, 0.8, 0.9$ , and  $1.0$  mol%) lithium-niobium-tellurite glass samples, were measured under 374 nm excitation, as shown in Fig. 15. The average decay lifetimes of TNLC- $p$ Tb0.5Sm ( $p = 0, 0.6, 0.7, 0.8, 0.9$ , and  $1.0$  mol%) lithium-niobium-tellurite glass samples were calculated, as presented in Table 5. The decay lifetimes of  $\text{Sm}^{3+}$  at 601 nm, corresponding to  $^4\text{G}_{5/2} \rightarrow ^6\text{H}_{7/2}$  transition of  $\text{Sm}^{3+}$  ions<sup>32,33</sup> in these glass samples under 374 nm excitation were found to decrease with increasing  $\text{Tb}^{3+}$  concentration in the glass samples, further proving ET from  $\text{Sm}^{3+}$  to  $\text{Tb}^{3+}$  ions.<sup>33,34,39,40</sup>

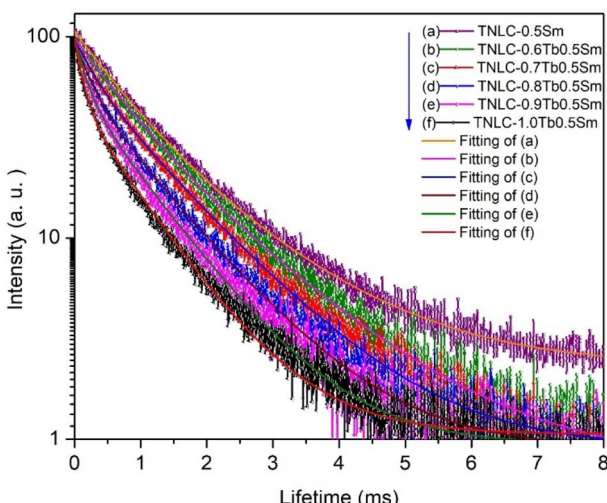


**Fig. 15** Decay lifetimes of  $\text{Sm}^{3+}$  at the  $^4\text{G}_{5/2} \rightarrow ^6\text{H}_{5/2}$  transition in TNLC- $p$ Tb0.5Sm ( $p = 0, 0.6, 0.7, 0.8, 0.9$ , and  $1.0$  mol%) glass samples under 374 nm excitation.

To evaluate the energy transfer efficiency (ETE) between  $\text{Tb}^{3+}$  and  $\text{Sm}^{3+}$  ions, we carried out ETE calculations for these ET processes. The ETE from  $\text{Tb}^{3+}$  to  $\text{Sm}^{3+}$  ions is denoted as  $\eta_{\text{ET}(\text{Tb} \rightarrow \text{Sm})}$  and was estimated using the luminescence lifetimes of the donor ( $\text{Tb}^{3+}$ ) in the presence and absence of the acceptor ( $\text{Sm}^{3+}$ ), according to the following equation:

$$\eta_{\text{ET}(\text{Tb} \rightarrow \text{Sm})} = 1 - \frac{\tau_{\text{Tb-Sm}}}{\tau_{\text{Tb}}}, \quad (7)$$

where  $\tau_{\text{Tb}}$  is the luminescence lifetime of  $\text{Tb}^{3+}$  ions in the absence of  $\text{Sm}^{3+}$  ions, and  $\tau_{\text{Tb-Sm}}$  is the luminescence lifetime of  $\text{Tb}^{3+}$  ions in the presence of  $\text{Sm}^{3+}$  ions (*i.e.* when energy transfer occurs).

Similarly, the ETE from  $\text{Sm}^{3+}$  to  $\text{Tb}^{3+}$  ions is denoted as  $\eta_{\text{ET}(\text{Sm} \rightarrow \text{Tb})}$  and was estimated using the luminescence lifetimes of the donor ( $\text{Sm}^{3+}$ ) in the presence and absence of the acceptor ( $\text{Tb}^{3+}$ ), according to the following equation:

$$\eta_{\text{ET}(\text{Sm} \rightarrow \text{Tb})} = 1 - \frac{\tau_{\text{Sm-Tb}}}{\tau_{\text{Sm}}}, \quad (8)$$

where  $\tau_{\text{Sm}}$  is the luminescence lifetime of  $\text{Sm}^{3+}$  ions in the absence of  $\text{Tb}^{3+}$  ions, and  $\tau_{\text{Sm-Tb}}$  is the luminescence lifetime of  $\text{Sm}^{3+}$  ions in the presence of  $\text{Tb}^{3+}$  ions. Based on the results presented in Table 5, we calculated ETE values to be 52.26% and 67.43% for the ET processes from  $\text{Tb}^{3+}$  to  $\text{Sm}^{3+}$  ions and from  $\text{Sm}^{3+}$  to  $\text{Tb}^{3+}$  ions, respectively.

## 4. Conclusions

In this study, a series of  $\text{Tb}^{3+}$ -doped,  $\text{Sm}^{3+}$ -doped,  $\text{Tb}^{3+}$ - $\text{Sm}^{3+}$  codoped, and  $\text{Tb}^{3+}$ - $\text{Sm}^{3+}$ - $\text{Yb}^{3+}$  tri-doped lithium-niobium-tellurite  $\text{TeO}_2$ - $\text{Nb}_2\text{O}_5$ - $\text{LiO}_2$ - $\text{CaO}$  glasses were synthesized *via* conventional melt-quenching. These glasses exhibited tunable multi-color emissions under excitation at 374 nm and 980 nm, which could be attributed to  $\text{Sm}^{3+}$  (yellow-pink),  $\text{Tb}^{3+}$  (yellowish-green), and  $\text{Yb}^{3+}$ -sensitized UC emissions of  $\text{Tb}^{3+}$ - $\text{Sm}^{3+}$ - $\text{Yb}^{3+}$  tri-doped glass materials. The DTA analysis showed the high thermal stability of the tri-doped glass, with  $\Delta T = 151$  °C, suitable for heat treatment and mechanical durability. The emission color could be effectively controlled by varying the  $\text{Sm}^{3+}$ - $\text{Tb}^{3+}$  concentrations and excitation wavelengths. The optimal  $\text{Tb}^{3+}$ / $\text{Sm}^{3+}$  molar ratio was 0.83 in the TNLC-0.5Tb0.6Sm sample for achieving CIE coordinates closest to white light emission. Spectral and lifetime measurements confirmed ETE between  $\text{Tb}^{3+}$  and  $\text{Sm}^{3+}$  ions. The combination of low phonon energy, high stability, emission tunability, and efficient ET highlights the potential of  $\text{Tb}^{3+}$ - $\text{Sm}^{3+}$  co-doped and  $\text{Tb}^{3+}$ - $\text{Sm}^{3+}$ - $\text{Yb}^{3+}$  tri-doped TNLC glasses for application in advanced color display and solid-state lighting devices, including WLEDs.

## Data availability

The authors confirm that the data supporting the findings of this study are available from the corresponding author upon request.

## Conflicts of interest

There are no conflicts of interest to declare.

## Acknowledgements

The corresponding author (Ho Kim Dan) would like to express his gratitude to Van Lang University.

## References

- 1 G. J. Li, M.-C. Tseng, Y. Chen, F. S.-Y. Yeung, H. Y. He, Y. C. Cheng, J. H. Cai and E. G. Chen, Color-conversion displays: current status and future outlook, *Light:Sci. Appl.*, 2024, **13**, 301, DOI: [10.1038/s41377-024-01618-8](https://doi.org/10.1038/s41377-024-01618-8).
- 2 J. C. Chen, Q. L. Zhao, B. H. Yu and U. Lemmer, A review on quantum dot-based color conversion layers for mini/micro-LED displays: Packaging, light management, and pixelation, *Adv. Opt. Mater.*, 2024, **12**, 2300873, DOI: [10.1002/adom.202300873](https://doi.org/10.1002/adom.202300873).
- 3 M. Vasilopoulou, A. R. B. M. Yusoff, M. Daboczi, J. Conforto, A. E. X. Gavim, W. J. D. Silva, A. G. Macedo, A. Soultati, G. Pistolis, F. K. Schneider, Y. F. Dong, P. Jacoutot, G. Rotas and J. Jang, High efficiency blue organic light-emitting diodes with below-bandgap electroluminescence, *Nat. Commun.*, 2021, **12**, 4868, DOI: [10.1038/s41467-021-25135-z](https://doi.org/10.1038/s41467-021-25135-z).
- 4 T. Q. Sheng, Z. L. Fu, X. J. Wang, S. H. Zhou, S. Y. Zhang and Z. W. Dai, Solvothermal synthesis and luminescence properties of BaCeF<sub>5</sub>, and BaCeF<sub>5</sub>: Tb<sup>3+</sup>, Sm<sup>3+</sup> Nanocrystals: An approach for white light emission, *J. Phys. Chem. C*, 2012, **36**(116), 19597–19603, DOI: [10.1021/jp306935k](https://doi.org/10.1021/jp306935k).
- 5 J. S. Alzahrani, Z. A. Alrowaili, A. V. Lebedev, I. O. Olarinoye, A. Hammoud, L. V. Vasileva and M. S. Al-Buraihi, Optical properties and radiation shielding performance of tellurite glassy composites: role of rare earth oxides, *Radiat. Phys. Chem.*, 2023, **212**, 111168, DOI: [10.1016/j.radphyschem.2023.111168](https://doi.org/10.1016/j.radphyschem.2023.111168).
- 6 J. E. Stanworth, Tellurite glasses, *Nature*, 1952, **169**, 581–582, DOI: [10.1038/169581b0](https://doi.org/10.1038/169581b0).
- 7 R. El-Mallawany, The optical properties of tellurite glasses, *J. Appl. Phys.*, 1992, **72**, 1774–1777, DOI: [10.1063/1.351649](https://doi.org/10.1063/1.351649).
- 8 J. Lousteau, D. Milanese, S. Abrate, N. Boetti, M. Pittarelli, S. Barbero and M. Ferrari, Exploring the influence of ZnF<sub>2</sub> on zinc-tellurite glass: unveiling changes in OH content, structure, and optical properties, *ACS Omega*, 2023, **8**(38), 35266–35274, DOI: [10.1021/acsomega.3c05010](https://doi.org/10.1021/acsomega.3c05010).
- 9 J. Biswas, S. Jana and S. Ghosh, Investigation on luminescence characteristics of Dy<sup>3+</sup>-Tb<sup>3+</sup> co-doped phospho-tellurite glasses for tunable green/white LED applications, *Spectrochim. Acta, Part A*, 2025, **331**, 125756, DOI: [10.1016/j.saa.2025.125756](https://doi.org/10.1016/j.saa.2025.125756).
- 10 V. K. Rai, S. B. Rai and D. K. Rai, Optical properties of Tb<sup>3+</sup> doped tellurite glass, *J. Mater. Sci.*, 2004, **39**, 4971–4975, DOI: [10.1023/B:JMSC.0000035348.82074.0a](https://doi.org/10.1023/B:JMSC.0000035348.82074.0a).
- 11 K. S. Rudramamba, S. K. Taherunnisa, D. V. K. Reddy, N. Veeraiah and M. R. Reddy, The structural and warm light emission properties of Sm<sup>3+</sup>/Tb<sup>3+</sup> doubly doped strontium bismuth borosilicate glasses for LED applications, *Spectrochim. Acta, Part A*, 2019, **220**, 117097, DOI: [10.1016/j.saa.2019.05.002](https://doi.org/10.1016/j.saa.2019.05.002).
- 12 M. Vijayakumar and K. Marimuthu, Effect of Tb<sup>3+</sup> concentration on Sm<sup>3+</sup> doped leadfluoro-borophosphate glasses for WLED applications, *J. Non-Cryst. Solids*, 2016, **447**, 45–54, DOI: [10.1016/j.jnoncrysol.2016.05.028](https://doi.org/10.1016/j.jnoncrysol.2016.05.028).
- 13 G. Lakshminarayana, A. N. Meza-Rocha, O. Soriano-Romero, E. F. Huerta, U. Caldiño, A. Lira, D.-E. Lee, J. H. Yoon and T. J. Park, Analysis of fluorescence characteristics of Sm<sup>3+</sup>-doped B<sub>2</sub>O<sub>3</sub>-rich glasses for Orange-light-emitting diodes, *J. Alloys Compd.*, 2021, **884**, 161076, DOI: [10.1016/j.jallcom.2021.161076](https://doi.org/10.1016/j.jallcom.2021.161076).
- 14 A. U. Trápala-Ramírez, J. L. N. Gálvez-Sandoval, A. Lira, I. Camarillo, E. Alvarez-Ramos, A. N. Meza-Rocha and U. Caldiño, Calcium-zinc phosphate glasses activated with Tb<sup>3+</sup>/Eu<sup>3+</sup> for laser and white LED applications, *J. Lumin.*, 2019, **215**, 116621, DOI: [10.1016/j.jlumin.2019.116621](https://doi.org/10.1016/j.jlumin.2019.116621).
- 15 H. K. Dan, D. C. Zhou, R. F. Wang, Q. Jiao, Z. W. Yang, Z. G. Song, X. Yu and J. B. Qiu, Effect of Mn<sup>2+</sup> ions on the enhancement upconversion emission and energy transfer of Mn<sup>2+</sup>/Tb<sup>3+</sup>/Yb<sup>3+</sup> tri-doped transparent glass-ceramics, *Mater. Lett.*, 2015, **150**, 76–80, DOI: [10.1016/j.matlet.2015.03.005](https://doi.org/10.1016/j.matlet.2015.03.005).
- 16 P. X. Le, N. M. Ty, J. B. Qiu, D. C. Zhou and H. K. Dan, Enhanced upconversion and near-infrared emissions of co-doped Ho<sup>3+</sup>/Yb<sup>3+</sup> in TeO<sub>2</sub>-ZnO-Na<sub>2</sub>CO<sub>3</sub>-La<sub>2</sub>O<sub>3</sub> tellurite glasses, *Opt. Mater. Express*, 2019, **9**, 3998–4008, DOI: [10.1364/OME.9.003998](https://doi.org/10.1364/OME.9.003998).
- 17 A. Roy, A. Dwivedi, H. Mishra, A. K. Rai and S. B. Rai, Generation of color tunable emissions from Ho<sup>3+</sup>/Tm<sup>3+</sup>/Yb<sup>3+</sup> co-doped YTaO<sub>4</sub> phosphors through NIR excitation under different conditions (variation of concentration, excitation pump power and the external temperature), *J. Alloys Compd.*, 2021, **865**, 158938, DOI: [10.1016/j.jallcom.2021.158938](https://doi.org/10.1016/j.jallcom.2021.158938).
- 18 P. Dharmaiah, C. S. Dwaraka Viswanath, C. Basavapoornima, K. V. Krishnaiah, C. K. Jayasankar and S.-J. Hong, Luminescence and energy transfer in Dy<sup>3+</sup>/Tb<sup>3+</sup> co-doped transparent oxyfluorosilicate glass-ceramics for green emitting applications, *Mater. Res. Bull.*, 2016, **83**, 507–514, DOI: [10.1016/j.materresbull.2016.06.044](https://doi.org/10.1016/j.materresbull.2016.06.044).
- 19 H. K. Dan, N. D. Trung, T. H. Le, N. L. Thai, N. M. Ty, D. C. Zhou and J. B. Qiu, Influence of F<sup>-</sup> on the reduction process of Eu<sup>3+</sup> to Eu<sup>2+</sup> and optical properties of Eu<sup>3+</sup>/Eu<sup>2+</sup>-Er<sup>3+</sup>-Yb<sup>3+</sup> co-doped niobate silicate glasses, *J. Non-Cryst. Solids*, 2022, **581**, 121417, DOI: [10.1016/j.jnoncrysol.2022.121417](https://doi.org/10.1016/j.jnoncrysol.2022.121417).
- 20 J. Dahiya, A. Hooda, A. Agarwal and S. Khasa, Effect of Dysprosium and Samarium RE ion co-doping on photoluminescence behaviour of novel alkali fluoride bismuth borate glasses: A white LED material, *Opt. Mater.*, 2022, **134**, 113162, DOI: [10.1016/j.optmat.2022.113162](https://doi.org/10.1016/j.optmat.2022.113162).
- 21 F. Nawaz, M. R. Sahar and S. K. Ghoshal, The influence of Yb co-doping on optical properties of Sm-doped sodium tellurite glasses, *Adv. Mater. Res.*, 2014, **895**, 359–362, DOI: [10.4028/www.scientific.net/AMR.895](https://doi.org/10.4028/www.scientific.net/AMR.895).
- 22 J. Li, D. Zhang, Y. X. Wu, L. L. Li, X. L. Zhang, S. Q. Xu and J. J. Zhang, Multi-color afterglow of the LiGa<sub>5</sub>O<sub>8</sub>: Tb<sup>3+</sup>/Sm<sup>3+</sup> co-doped gallosilicate glass *via* energy transfer and trap



sharing for optical anti-counterfeiting, *J. Mater. Chem. C*, 2024, **12**, 15733–15738, DOI: [10.1039/D4TC03171G](https://doi.org/10.1039/D4TC03171G).

23 N. Elkhoshkhany, R. Essam and E. Sayed Yousef, Influence of  $\text{La}_2\text{O}_3$  on the structural, optical and thermal properties of  $\text{TeO}_2\text{-ZnO-Li}_2\text{O-Nb}_2\text{O}_5$  glass, *J. Non-Cryst. Solids*, 2020, **536**, 119994, DOI: [10.1016/j.jnoncrysol.2020.119994](https://doi.org/10.1016/j.jnoncrysol.2020.119994).

24 N. Elkhoshkhany, S. Y. Marzouk, N. Moataz and S. H. Kandil, Structural and optical properties of  $\text{TeO}_2\text{-Li}_2\text{O-ZnO-Nb}_2\text{O}_5\text{-Er}_2\text{O}_3$  glass system, *J. Non-Cryst. Solids*, 2018, **500**, 289–301, DOI: [10.1016/j.jnoncrysol.2018.08.011](https://doi.org/10.1016/j.jnoncrysol.2018.08.011).

25 H. Benrejeb, K. Soler-Carracedo, A. D. Lozano-Gorrín, S. Hraiech and I. R. Martin, Energy transfer studies in  $\text{Tb}^{3+}\text{-Yb}^{3+}$  co-doped phosphate glasses, *Mater.*, 2021, **14**(22), 6782, DOI: [10.3390/ma14226782](https://doi.org/10.3390/ma14226782).

26 H. K. Dan, N. M. Ty, V. H. Nga, D. T. Phuc, A.-L. Phan, D. C. Zhou and J. B. Qiu, Broadband flat near-infrared emission and energy transfer of  $\text{Pr}^{3+}\text{-Er}^{3+}\text{-Yb}^{3+}$  tri-doped niobate tellurite glasses, *J. Non-Cryst. Solids*, 2020, **549**, 120335, DOI: [10.1016/j.jnoncrysol.2020.120335](https://doi.org/10.1016/j.jnoncrysol.2020.120335).

27 D. C. Zhou, R. F. Wang, Z. W. Yang, Z. G. Song, Z. Y. Yin and J. B. Qiu, Spectroscopic properties of  $\text{Tm}^{3+}$  doped  $\text{TeO}_2\text{-R}_2\text{O-La}_2\text{O}_3$  glasses for 1.47  $\mu\text{m}$  optical amplifiers, *J. Non-Cryst. Solids*, 2011, **357**, 2409–2412, DOI: [10.1016/j.jnoncrysol.2010.12.027](https://doi.org/10.1016/j.jnoncrysol.2010.12.027).

28 R. El-Mallawany, Tellurite glasses Part 2. Anelastic, phase separation, Debye temperature and thermal properties, *Mater. Chem. Phys.*, 1999, **60**, 103–131, DOI: [10.1016/S0254-0584\(99\)00082-6](https://doi.org/10.1016/S0254-0584(99)00082-6).

29 G. V. Prakash, D. N. Rao and A. K. Bhatnagar, Linear optical properties of niobium-based tellurite glass, *Solid State Commun.*, 2001, **119**(1), 39–44, DOI: [10.1016/S0038-1098\(01\)00195-8](https://doi.org/10.1016/S0038-1098(01)00195-8).

30 H. K. Dan, N. M. Ty, T. D. Tap, D.-N. Le, L. T. Vinh, D. C. Zhou and J. B. Qiu, Energy transfer and spectroscopic properties of  $\text{Cr}^{3+}\text{/Yb}^{3+}$  co-doped  $\text{TeO}_2\text{-ZnO-La}_2\text{O}_3$  tellurite glasses under different wavelength excitation lights, *Opt. Mater.*, 2020, **100**, 109662, DOI: [10.1016/j.optmat.2020.109662](https://doi.org/10.1016/j.optmat.2020.109662).

31 H. K. Dan, D. C. Zhou, R. F. Wang, T. M. Hau, Q. Jiao, Z. W. Yang, Z. G. Song, X. Yu and J. B. Qiu, Energy transfer and upconversion emission of  $\text{Tm}^{3+}\text{/Tb}^{3+}\text{/Yb}^{3+}$  co-doped transparent glass-ceramics containing  $\text{Ba}_2\text{LaF}_7$  nanocrystals, *J. Non-Cryst. Solids*, 2013, **378**, 181–185, DOI: [10.1016/j.jnoncrysol.2013.07.006](https://doi.org/10.1016/j.jnoncrysol.2013.07.006).

32 C. Jin, J. Zhang, W. D. Lu and Y. T. Fei, Tunable luminescence of  $\text{LiY}_9(\text{SiO}_4)_6\text{O}_2\text{:Ce}^{3+}\text{-Tb}^{3+}\text{-Sm}^{3+}$  phosphors for LED and temperature-sensing applications, *J. Lumin.*, 2019, **214**, 116581, DOI: [10.1016/j.jlumin.2019.116581](https://doi.org/10.1016/j.jlumin.2019.116581).

33 Y. N. Guo, Q. W. Wang, X. Y. Zhao, L. P. Wang, Y. Wan, H. Zhang and C. Su, Preparation and luminescence properties of  $\text{Tb}^{3+}\text{-Sm}^{3+}$  co-doped  $\text{K}_3\text{Gd}(\text{PO}_4)_2$  crystalline glass ceramics, *Opt. Mater.*, 2024, **148**, 114830, DOI: [10.1016/j.optmat.2024.114830](https://doi.org/10.1016/j.optmat.2024.114830).

34 Le-Q. Yao, G.-H. Chen, T. Yang, Y. Luo and Y. Yang, Optical properties and energy transfer in  $\text{Tb}^{3+}\text{/Sm}^{3+}$  co-doped  $\text{Na}_2\text{O-CaO-P}_2\text{O}_5\text{-B}_2\text{O}_3\text{-ZrO}_2$  glasses, *J. Alloys Compd.*, 2017, **692**, 346–350, DOI: [10.1016/j.jallcom.2016.09.053](https://doi.org/10.1016/j.jallcom.2016.09.053).

35 H. K. Dan, A. L. Phan, N. M. Ty, D. C. Zhou and J. B. Qiu, Optical bandgaps and visible/near-infrared emissions of  $\text{Bi}^{n+}$ -doped ( $n = 1, 2$ , and 3) fluoroaluminosilicate glasses via  $\text{Ag}^+\text{-K}^+$  ions exchange process, *Opt. Mater.*, 2021, **112**, 110762, DOI: [10.1016/j.optmat.2020.110762](https://doi.org/10.1016/j.optmat.2020.110762).

36 P. T. Phong, P. H. Nam, N. X. Phuc, B. T. Huy, L. T. Lu, D. H. Manh and I.-J. Lee, Effect of zinc concentration on the structural, optical, and magnetic properties of mixed Co-Zn ferrites nanoparticles synthesized by low-temperature hydrothermal method, *Metall. Mater. Trans. A*, 2019, **50**, 1571–1581, DOI: [10.1007/s11661-018-5096-z](https://doi.org/10.1007/s11661-018-5096-z).

37 K. A. Kumar, S. Babu, V. R. Prasad, S. Damodaraiah and Y. C. Ratnakaram, Optical response and luminescence characteristics of  $\text{Sm}^{3+}$  and  $\text{Tb}^{3+}\text{/Sm}^{3+}$  co-doped potassium-fluoro-phosphate glasses for reddish-orange lighting applications, *Mater. Res. Bull.*, 2017, **90**, 31–40, DOI: [10.1016/j.materresbull.2017.01.046](https://doi.org/10.1016/j.materresbull.2017.01.046).

38 V. Lakkamraju, K. N. Kumar and H. Pyung, Unravelling the process of energy transfer and color tuning from warm to cool white light emission in (Tb/Sm): lithium borate glasses, *Opt. Lett.*, 2019, **44**(20), 5029–5032, DOI: [10.1364/OL.44.005029](https://doi.org/10.1364/OL.44.005029).

39 C. G. Pérez-Hernández, R. Sánchez-Zeferino, U. Salazar-Kuri and M. E. Álvarez-Ramos, Fabrication, structural properties, and tunable light emission of  $\text{Sm}^{3+}\text{-Tb}^{3+}$  co-doped  $\text{SrSnO}_3$  perovskite nanoparticles, *Chem. Phys.*, 2021, **551**, 111324, DOI: [10.1016/j.chemphys.2021.111324](https://doi.org/10.1016/j.chemphys.2021.111324).

40 A. Bahadur, R. S. Yadav, R. V. Yadav and S. B. Rai, Multimodal emissions from  $\text{Tb}^{3+}\text{/Yb}^{3+}$  co-doped lithium borate glass: upconversion, downshifting and quantum cutting, *J. Solid State Chem.*, 2017, **246**, 81–86, DOI: [10.1016/j.jssc.2016.11.004](https://doi.org/10.1016/j.jssc.2016.11.004).

41 S. Pandey, A. Pandey and V. K. Rai, Synthesis and Characterization of  $\text{Sm}^{3+}\text{-Yb}^{3+}$  codoped  $\text{Y}_2\text{O}_3$  Phosphor, *J. Disp. Technol.*, 2013, **9**(12), 989–994. [https://doi.org/10.1016/S0038-1098\(01\)00195-8](https://doi.org/10.1016/S0038-1098(01)00195-8).

42 T. T. Hong, P. D. H. Yen, V. X. Quang and P. T. Dung, Luminescence properties of Ce/Tb/Sm co-doped tellurite glass for white LEDs application, *Mater. Trans.*, 2015, **56**(9), 1419–1421, DOI: [10.2320/matertrans.MA201509](https://doi.org/10.2320/matertrans.MA201509).

43 Y. Z. Jiang, H. P. Xia, L. Fu, J. Z. Zhang, S. Yang, X. M. Gu, J. L. Zhang, Y. P. Zhang, D. J. Wang, H. C. Jiang and B. J. Chen, Growth and Optical Spectra of  $\text{Tb}^{3+}\text{/Sm}^{3+}\text{/Ce}^{3+}$  Triply doped  $\text{LiYF}_4$  single crystals for White-Light LEDs, *Nanosci. Nanotechnol.*, 2016, **16**, 1532–1536, DOI: [10.1166/jnn.2016.10803](https://doi.org/10.1166/jnn.2016.10803).

44 X. K. Sun, Z. Z. Huang, Y. H. Guo, S. H. Zhou and K. L. Liu,  $\text{Tb}^{3+} \rightarrow \text{Sm}^{3+}$  energy transfer induced tunable luminescence in  $\text{Ba}_3\text{MgSi}_2\text{O}_8\text{:Tb}^{3+}\text{/Sm}^{3+}$  phosphors, *J. Lumin.*, 2020, **219**, 116925, DOI: [10.1016/j.jlumin.2019.116925](https://doi.org/10.1016/j.jlumin.2019.116925).

45 A. N. Meza-Rocha, G. Muñoz H, A. Speghini, M. Bettinelli and U. Caldiño, Neutral and warm white light emission in  $\text{Tb}^{3+}\text{/Sm}^{3+}$  zinc phosphate glasses, *Opt. Mater.*, 2015, **47**, 537–542, DOI: [10.1016/j.optmat.2015.06.035](https://doi.org/10.1016/j.optmat.2015.06.035).

46 N. F. Andrade Neto, J. M. P. Silva, R. L. Tranquillin, E. Longo, J. F. M. Domeneguetti, M. R. D. Bomio and F. V. Motta, Photoluminescent properties of  $\text{Sm}^{3+}$  and  $\text{Tb}^{3+}$  codoped



CaWO<sub>4</sub> nanoparticles obtained by a one-step sonochemical method, *J. Mater. Sci.: Mater. Electron.*, 2020, **31**, 13261–13272, DOI: [10.1007/s10854-020-03878-7](https://doi.org/10.1007/s10854-020-03878-7).

47 K. Nie, R. R. Zhou, C.-A. Cheng, X. Q. Duan, Z. Y. Hu, L. F. Mei, H. K. Liu, L. X. Wang, H. Wang and X. X. Ma, Tb<sup>3+</sup> and Sm<sup>3+</sup> co-doped Ca<sub>2</sub>La<sub>3</sub>(SiO<sub>4</sub>)<sub>3</sub>F phosphor: Synthesis, color regulation, and luminescence properties, *RSC Adv.*, 2022, **12**, 33200–33206, DOI: [10.1039/D2RA06648C](https://doi.org/10.1039/D2RA06648C).

48 B. Yuan, J. X. Gou, C. C. Qi, L. Kong, M. Y. Qu, G. Y. Luan and X. T. Zhang, Energy transfer for Ce<sup>3+</sup>/Tb<sup>3+</sup>/Sm<sup>3+</sup> induced bright white emission in single-phase CaLa<sub>4</sub>(SiO<sub>4</sub>)<sub>3</sub>O: Ce<sup>3+</sup>, Tb<sup>3+</sup>, Sm<sup>3+</sup> phosphors and their application in white-light-emitting diodes, *RSC Adv.*, 2024, **14**, 7061–7072, DOI: [10.1039/D4RA00443D](https://doi.org/10.1039/D4RA00443D).

49 Y. N. Guo, Q. W. Wang, X. Y. Zhao, L. P. Wang, Y. C. Wan, H. B. Zhang and C. H. Su, Preparation and luminescence properties of Tb<sup>3+</sup>-Sm<sup>3+</sup> co-doped K<sub>3</sub>Gd(PO<sub>4</sub>)<sub>2</sub> crystalline glass ceramics, *Opt. Mater.*, 2024, **148**, 114830, DOI: [10.1016/j.optmat.2024.114830](https://doi.org/10.1016/j.optmat.2024.114830).

50 E. J. Ansari, S. Patle, A. R. Pusdekar, N. S. Ugemuge and A. Selokar, Structural and spectroscopic analysis of K<sub>2</sub>Y(WO<sub>4</sub>)(PO<sub>4</sub>): Sm<sup>3+</sup>, Tb<sup>3+</sup> phosphors for optical applications, *Spectrochim. Acta Part A Mol. Spectrosc.*, 2025, 126269, DOI: [10.1016/j.saa.2025.126269](https://doi.org/10.1016/j.saa.2025.126269), <https://www.sciencedirect.com/journal/spectrochimica-acta-part-a>

**molecular-and-biomolecular-spectroscopy/vol/339/suppl/C339.**

51 O. Soriano-Romero, E. F. Huerta, A. N. Meza-Rocha and U. Caldiño, Orange and yellow emissions through Sm<sup>3+</sup> and Tb<sup>3+</sup>/Sm<sup>3+</sup> doped potassium-zinc phosphate glasses for WLED applications, *Ceram. Interfaces*, 2023, **49**, 36353–36359, DOI: [10.1016/j.ceramint.2023.08.319](https://doi.org/10.1016/j.ceramint.2023.08.319).

52 J. Hernández-Andrés, R. L. Lee and J. Romero, Calculating correlated color temperatures across the entire gamut of daylight and skylight chromaticities, *Appl. Opt.*, 1999, **38**(27), 5703–5709, DOI: [10.1364/AO.38.005703](https://doi.org/10.1364/AO.38.005703).

53 M. E. Alvarez-Ramos, J. Alvarado-Rivera, M. E. Zayas, U. Caldiño and J. Hernández-Paredes, Yellow to orange-reddish glass phosphors: Sm<sup>3+</sup>, Tb<sup>3+</sup> and Sm<sup>3+</sup>/Tb<sup>3+</sup> in zinc tellurite-germanate glasses, *Opt. Mater.*, 2018, **112**, 88–93, DOI: [10.1016/j.optmat.2017.09.033](https://doi.org/10.1016/j.optmat.2017.09.033).

54 X. S. Qiao, X. P. Fan, Z. Xue and X. H. Xu, Short-wavelength upconversion luminescence of Yb<sup>3+</sup>/Tm<sup>3+</sup> co-doped glass ceramic containing SrF<sub>2</sub> nanocrystals, *J. Non-Cryst. Solids*, 2011, **357**(1), 83–87, DOI: [10.1016/j.jnoncrysol.2010.09.008](https://doi.org/10.1016/j.jnoncrysol.2010.09.008).

55 D. T. Khan, N. T. Dang, S. H. Jabarov, T. G. Naghiyev, R. M. Rzayev, T. Q. Nguyen, H. V. Tuyen, N. T. Thanh and L. V. T. Son, Study on luminescent properties of Tb<sup>3+</sup> and Sm<sup>3+</sup> co-doped CaSiO<sub>3</sub> phosphors for white light emitting diodes, *Mater. Res. Express*, 2020, **7**, 016507, DOI: [10.1088/2053-1591/ab5ab8](https://doi.org/10.1088/2053-1591/ab5ab8).

